微细电火花线切割加工表面耐蚀性的试验分析

张 彬[1,2]， 郭黎滨[1]， 崔 海[1,3]， 张慧刚[1]
(1. 哈尔滨工程大学 机电工程学院，哈尔滨 150001；2. 哈尔滨工程大学 图书馆，哈尔滨 150001；
3. 哈尔滨工程大学 工程训练中心，哈尔滨 150001)

摘 要：为了了解不同材料在微细电火花线切割(MWEDM)加工下的表面耐蚀性，分别对W18Cr4V，60Si2Mn和M42三种材料进行加工，借助微电解池装置和电化学工作站对各试件做表面耐蚀性试验，进行电化学阻抗谱和动电位极化曲线测量分析，采用倒置金相显微镜对腐蚀后的表面进行拍照观察并与平磨加工表面进行对比. 结果表明，微细电火花线切割加工表面耐蚀性整体优于平磨加工表面；对于不同材料，MWEDM表面耐蚀性存在显著差异；对于同种材料，选取适当的加工参数能够得到耐蚀性较好的表面.

关键词：微细电火花线切割；耐蚀性；阻抗谱；极化曲线
中图分类号：TG 661 **文献标识码**：A **文章编号**：0253－360X(2014)11－0093－04

0 序 言

微细电火花线切割加工(micro wire electrical discharge machining，MWEDM)是实现超精、微细加工行之有效的方法之一，其以独特的加工方法以及较高的性价比得到了迅速的发展，并在许多微型机械生产领域发挥了重要的作用. 加工过程中，通常采用微细的钨或其它材料的电极丝(直径为10～50 μm)进行放电切割，主要用于加工尺寸在0.1～1 mm的零件[1,2]. 由于MWEDM是在线电极与工件之间随机产生微细电火花，将电能转化成热能进行加工，当工件经MWEDM后，工件表面会出现由无方向性的无数小凹坑和硬凸起组成的放电凹坑，其表面微观形貌与纹理构造与切削加工表面存在极大差别. 由于表面微观形貌对工件表面的耐蚀性有很大影响，而工件的耐蚀性是其使用性能好坏和寿命长短的关键因素之一，所以对MWEDM表面耐蚀性的研究势在必行[3,4].

目前国内外对微细电火花的研究主要集中在机床设备和工艺规律两个方面，尚无对其加工工件耐蚀性方面的研究. 因此，对工程中三种常用材料，采用不同的加工参数进行MWEDM，然后分别进行电化学阻抗谱和动电位极化曲线测量分析，对腐蚀后的表面进行倒置金相显微镜观察，从而对MWEDM表面耐蚀性有更加深入的认识.

收稿日期：2014－09－28
基金项目：黑龙江省自然科学基金面上项目(E201137)

1 试验方法

1.1 试验材料

MWEDM加工是利用两极间脉冲火花放电产生大量的热能，熔化、蒸发和抛出工件电极材料，从而达到加工目的. 不同加工材料的物理化学特性，对加工的难易程度以及加工表面的质量有直接影响. 因此，试验选择了三种工程上适合特种加工的常用材料，分别是通用高速钢W18Cr4V、弹簧钢60Si2Mn和模具钢M42.

1.2 试件制作

对三种材料的试件，用MWEDM方法加工出4个面，其余面用平磨方法进行加工. 采用图1所示的标记方法对试件测试表面进行标记，各试件均加工出一个拐角缺口，方便辨认. 在图1中，Area1是

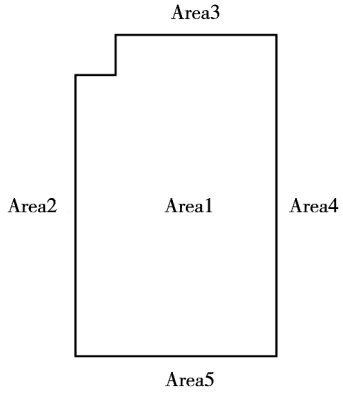

图1 试件测试表面标记方法
Fig. 1 Marking method of specimen testing surfaces

试件上表面，为平磨加工表面，Area2 ~ Area5 分别为采用不同参数进行 MWEDM 加工的四个表面.

采用哈尔滨工业大学研制的 HIT100 型微细电火花线切割机床对试件进行加工，电极钨丝为 Φ30 μm，对于三种材料在加工时分别采用不同的电加工参数. 材料 W18Cr4V 的试件尺寸为 1 mm × 1.5 mm，加工波形为方波，脉冲宽度 0.5 μs，脉冲时间 5 μs. 其余参数如表 1 所示.

表 1 W18Cr4V 试件的加工参数

Table 1 Machining parameter of test specimen W18Cr4V

表面序号	电容 C/pF	电压 U/V	电阻 R/Ω	伺服系数 α	加工时间 t/min
Area2	500	80	2 400	0.9	142
Area3	500	60	1 200	0.5	56
Area4	1 000	110	400	0.5	41
Area5	1 000	50	1 600	0.9	158

材料 60Si2Mn 的试件尺寸为 1.1 mm × 1.4 mm，加工波形为方波，脉冲宽度 2 μs，脉冲时间 20 μs，其余参数如表 2 所示.

表 2 60Si2Mn 试件的加工参数

Table 2 Machining parameter of test specimen 60Si2Mn

表面序号	电容 C/pF	电压 U/V	电阻 R/Ω	伺服系数 α	加工时间 t/min
Area2	2 500	90	800	0.3	47
Area3	3 000	50	3 200	0.3	80
Area4	2 500	110	2 000	0.7	55
Area5	3 000	80	800	0.7	57

材料 M42 的试件尺寸为 1.1 mm × 1.4 mm，加工波形为方波，脉宽 2 μs，脉间 20 μs，其余参数如表 3 所示.

表 3 M42 试件的加工参数

Table 3 Machining parameter of test specimen M42

表面序号	电容 C/pF	电压 U/V	电阻 R/Ω	伺服系数 α	加工时间 t/min
Area2	2 500	90	800	0.3	47
Area3	3 000	50	3 200	0.3	77
Area4	2 500	110	2 000	0.7	55
Area5	3 000	80	800	0.7	43

1.3 试验仪器和参数

试验采用经典的三电极体系，使用自制的微电解池装置对试件进行微区测试，用铂丝作为对电极，自制氧化 Ag/AgCl 为参比电极，测量溶液为 pH = 5 的 3.5% 的 NaCl 溶液，所用毛细管尖端直径约为 100 μm. 为防止其受干扰，将微电解池系统放在法拉第笼子中. 试验采用 Eco Chemie 公司生产的 AUTOLAB PGSTAT302 型电化学工作站进行电化学测试. 在电化学阻抗谱的测试中，测试的频率范围是 100 ~ 10 MHz，正弦波扰动信号的幅值为 10 mV，测试温度为室温. 在动电位极化曲线测量中，测试的电位从相对于开路电位 -0.3 V 开始，扫描速度为 5 mV/s. 为了更为直观地观察试件表面被腐蚀的情况，采用 LEICA DMILM 倒置金相显微镜对腐蚀后的表面进行拍照观察.

2 电化学阻抗谱分析

电化学阻抗谱是一种以小振幅的正弦波电位(或电流)为扰动信号的电化学测量方法，通过在很宽的频率范围内测量阻抗来研究电极系统，可以得到比其它常规的电化学方法更多的动力学信息及电极界面结构的信息.

对 W18Cr4V 试件、60Si2Mn 试件和 M42 试件，分别进行电化学阻抗谱测试，结果见图 2，横坐标为阻抗实部，纵坐标为阻抗虚部. 图 2a 为局部图，可以看出，Area5 的阻抗较大，即耐蚀性明显优于其它各面; Area1，Area2，Area3 和 Area4 的阻抗较小，耐蚀性较差. 图 2b 为局部图. 其中 Area1，Area 3 和 Area4 表现出的阻抗很小，其耐蚀性较差; Area5 的阻抗较大，则其耐蚀性较好; Area2 表现出的阻抗最大，其耐蚀性最好. 图 2c 中，Area1 表现出的阻抗值较大; Area2，Area3，Area4 和 Area5 的阻抗值差别不大，四个面之间相比无明显的优劣性. 可以看出，MWEDM 加工电参数对 M42 这种材料的耐蚀性影响不大.

3 动电位极化曲线分析

对 W18Cr4V 试件、60Si2Mn 试件和 M42 试件分别测量动电位极化曲线，得到结果见图 3，横坐标为电位，纵坐标为电流密度.

在图 3a 中，经过平磨加工的 Area1 完全不存在钝化区，为活性溶解状态，耐蚀性最差; 经过 MWEDM 的 Area2，Area3，Area4，Area5 均表现为钝化行为，其中 Area4 存在钝化区，但其维钝电流密度较大，耐蚀性相对处于中等; 而 Area2 和 Area5 则有明显的钝化区，其维钝电流密度也较小，耐蚀性较好.

在图 3b 中，Area1 有明显的钝化区域存在，但其

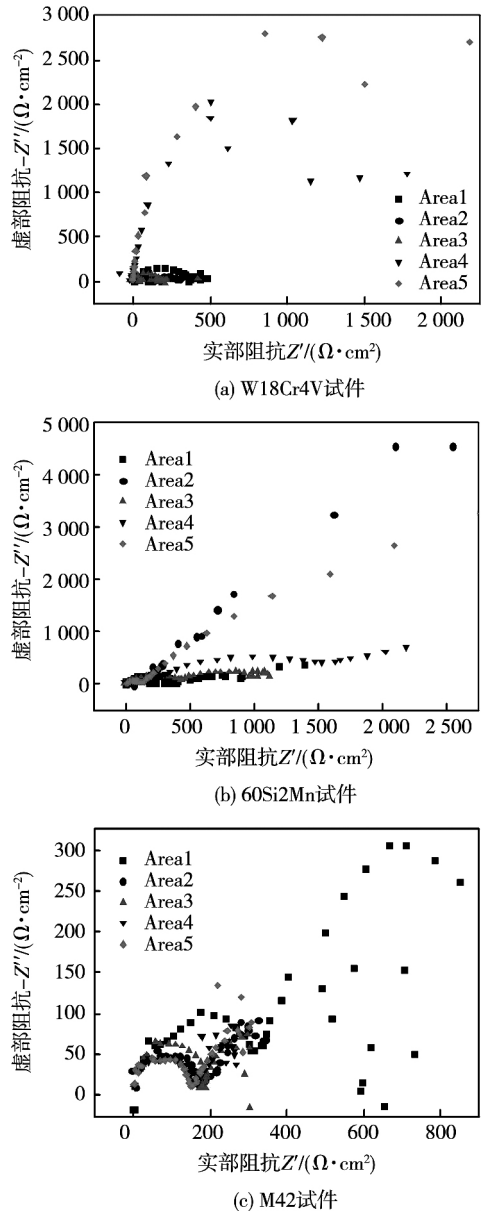

(a) W18Cr4V试件

(b) 60Si2Mn试件

(c) M42试件

图 2　试件的电化学阻抗谱

Fig. 2　EIS of test specimens

维钝电流密度较大. Area2 的维钝电流密度较小，其击破电位约在 0.06 V，其钝化区域宽度约为 500 mV. Area3 的阳极区为明显的活性溶解过程. Area4 的维钝电流密度较大，且击破电位较低. Area5 表现为钝化区域很窄的钝化行为. 可以看出，Area1，Area3 和 Area4 的耐蚀性较差; Area5 的维钝电流密度处在一个范围内，但都明显大于 Area2 的维钝电流密度，所以 Area2 的耐蚀性最好，这与电化学阻抗谱上的结果是相吻合的.

在图 3c 中，五个面均没有表现出明显的钝化区，且极化曲线几乎重合; 而从电流密度和电位分布情况来看，Area2 的耐蚀性略优于其它四面. 可以得出和电化学阻抗谱相似的结论: 不同的电加工参数对 M42 试件的耐蚀性影响不大，Area2 的 MWEDM 加工参数可优先选取.

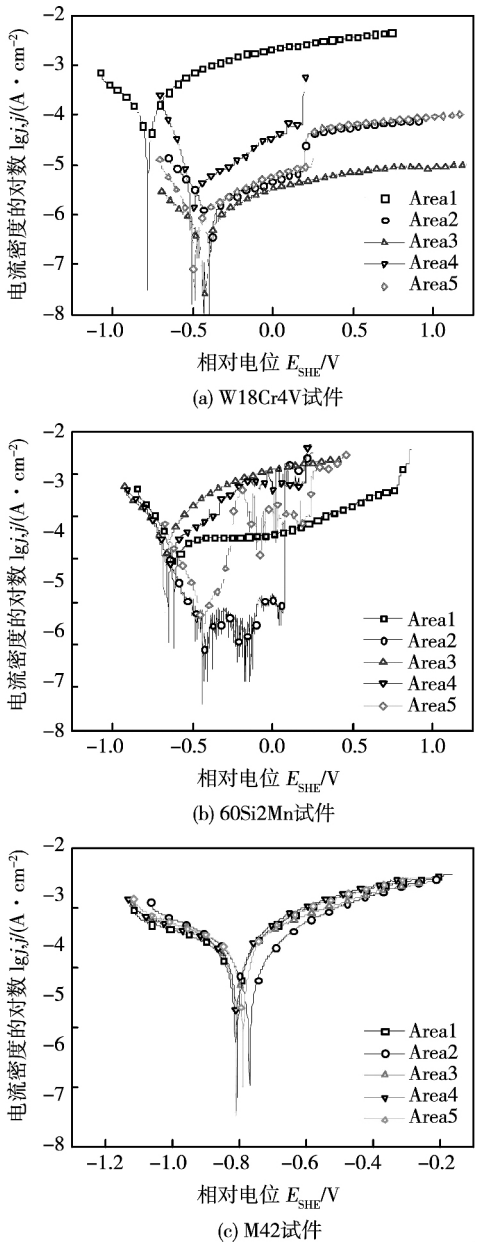

(a) W18Cr4V试件

(b) 60Si2Mn试件

(c) M42试件

图 3　试件的动电位极化曲线

Fig. 3　Potentiodynamic polarization curves of specimens

4　倒置金相显微镜下观察

为了更为直观的观察试件表面被腐蚀情况，试验中用 LEICA DMILM 倒置金相显微镜对腐蚀后的表面进行观察，见图 4.

图 4 选取的是被腐蚀得较为严重的表面形貌，图 4 中有明显暗坑处即为腐蚀试验测试点，与正常平面相比，可以清晰地观察到被腐蚀情况，得出的结论与上面的试验结果相吻合.

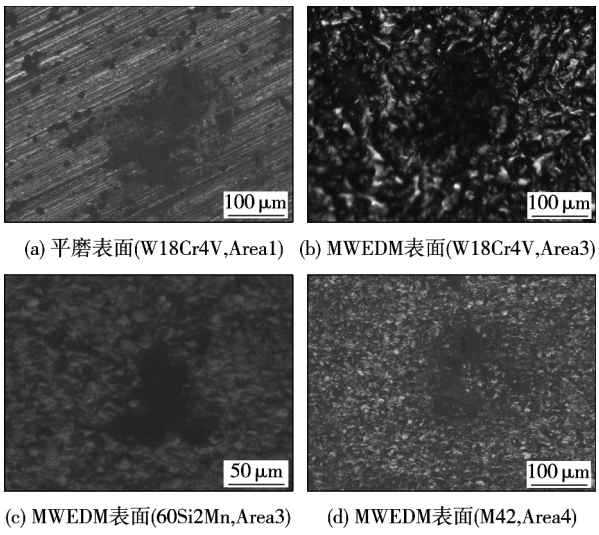

(a) 平磨表面(W18Cr4V,Area1) (b) MWEDM表面(W18Cr4V,Area3)

(c) MWEDM表面(60Si2Mn,Area3) (d) MWEDM表面(M42,Area4)

图 4 试样表面被腐蚀后的金相组织形貌

Fig. 4 Metallographic pictures of surfaces after corrosion

5 结 论

(1) 观察 W18Cr4V 试件五个测试表面的耐蚀性,可知平磨加工表面的耐蚀性最差. 在 60Si2Mn 试件的五个测试表面中,可以看出,只要选取适当的 MWEDM 放电能量,就可得到耐蚀性较好的加工表面. 对于 M42 试件的五个测试表面,其耐蚀性都不太好,但 MWEDM 表面的耐蚀性还是优于平磨加工表面. 试验可以看出,MWEDM 表面的耐蚀性整体优于平磨加工表面.

(2) 被测三种材料的耐蚀性由强到弱分别为:W18Cr4V 试件、60Si2Mn 试件、M42 试件. 对三种材料的所有测试表面耐蚀性观察,可知 W18Cr4V 试件各测试表面的耐蚀性普遍较高,而 M42 试件各测试表面的耐蚀性普遍较低,60Si2Mn 试件居中. 试验说明,不同材料的 MWEDM 表面,耐蚀性差异明显,实际应用中应依据使用功能选取适当的加工材料.

(3) 分别对三种试件的四个 MWEDM 表面的耐蚀性进行观察,不难发现,采用不同的加工电参数可以得到不同耐蚀性的加工表面. 随着放电能量的增加,加工表面的耐蚀性逐渐增强. 当达到最优状态后,放电能量的增加反而会导致加工表面耐蚀性急剧减弱.

参考文献:

[1] Guo L B, Zhang B, Cui H, *et al*. Research on corrosion resistance of MWEDM surface with different electrical parameters [J]. Applied Mechanics and Materials, 2012, 217/219: 1239 – 1242.

[2] Pham D T, Dimov S S, Bigot S, *et al*. Micro-EDM recent developments and research issues [J]. Journal of Materials Processing Technology, 2004, 149(1/3): 50 – 57.

[3] Zhang Z H, Gjuo L B, Cui H, *et al*. Surface texture evaluation of micro-WEDM [J]. Applied Mechanics and Materials, 2012, 138/189: 1251 – 1257.

[4] Ding H J, Guo L B, ZHANG Z H, *et al*. Study on fractal characteristic of surface micro-topography of micro-WEDM [J]. Applied Mechanics and Materials, 2009, 12/19: 1273 – 1277.

作者简介: 张 彬,男,1973 年出生,博士研究生,高级工程师. 主要从事特种加工和微细加工技术的研究. 发表论文 11 篇. Email: zhangbin@ hrbeu. edu. cn

[上接第 92 页]

[5] 李少青, 王学东, 张毓新, 等. 基于可编程控制的扫描电子束加工技术 [J]. 焊接学报, 2005, 26(7): 59 – 62, 66.
Li Shaoqing, Wang Xuedong, Zhang Yuxin, *et al*. Scanning electron beam processing technology based on programmable control [J]. Transactions of the China Welding Institution, 2005, 26(7): 59 – 62, 66.

作者简介: 韦寿祺,男,1964 出生,教授. 主要研究方向为电子束加工设备. 发表论文 50 余篇. Email: 13978340889@ 163. com

Metal and Electronic Material, General Research Institute for Nonferrous Metals, Beijing 100088, China). pp 75 – 78

Abstract: The optical microscope, scanning electron microscope (SEM) and electron back scattered diffraction (EBSD) were used to analyze the microstructure in different reigns of refill friction spot welded (RFSW) joints. The results showed that complete dynamic recrystallization occurred in the nugget zone with fine equiaxial grains, and much finer grains existed at the bottom. The nugget zone had no obvious texture. Part dynamic recrystallization occurred in the TMAZ which contained fine equiaxial grains and partly recovery grains with deformed structure. An obvious interface existed between the nugget zone and TMAZ, and its grain was much finer than those on both sides, and the grain boundary was denser.

Key words: refill friction spot welding; aluminium-lithium alloy; microstructure evolution; electron back scattered diffraction

Microstructure evolution after thermal exposure in weld interface of Ti_2AlNb/TC11 dual alloy forged at different temperatures JIA Qian[1,2], YAO Zekun[1,2], ZHANG Dongya[1,2], QIN Chun[1,2], TU Weijian[1,2], YANG Guobao[1,2], GENG Jingdong[3] (1. College of Materials Science and Engineering, Northwestern Polytechnical University, Xi'an 710072, China; 2. ERC of Forging Technique for Less Deformable Materials, Xi'an 710072, China; 3. Blade Factory of Guizhou Aero-Power Company, Pingba 561114, China). pp 79 – 83

Abstract: The microstructure evolution in Ti2AlNb/TC11 dual alloys after near thermal forging, gradient heat treatment and thermal exposure at 550 ℃ for 50 h and 100 h, respectively, was investigated with optical microscope (OM) and transmission electron microscope (TEM). The results show that B2→O + β decomposition occurred in the welded seam and Ti_2AlNb matrix, and α_2 phase migrated to the grain boundary of B2 during thermal exposure. The time for thermal exposure was longer, the segregation of α_2 phase at grain boundary was severer. And α_2 phase agglomerated into block when the thermal exposure time was 100 h. Also, the β phase grew coarse and its volume percentage increased simultaneously. If Al and Nb contents were large in the joint, α_2 phase would agglomerate at grain boundary, the original O phase overprinting with the secondary O phase decomposed from B2 phase would coarsen.

Key words: dual alloys; near thermal forging; thermal exposure; microstructure

Influence of weld strength match on distribution of stress triaxiality for aluminum alloy welded joint ZHU Hao[1,2], GUO Zhu[1,2], CUI Shaopeng[1,2], WANG Yanhong[1,2] (1. Hebei Provincial Key Laboratory of Traffic Engineering materials, Shijiazhuang TieDao University, Shijazhuang 050043, China; 2. School of Materials Science and Engineering, Shijiazhuang TieDao University, Shijazhuang 050043, China). pp 84 – 88

Abstract: The tensile simulation was carried out on 6063 aluminum alloy welded joint with different weld strength matches with software ABAQUS, and the influence of weld strength match on the distribution of stress triaxiality in aluminum alloy welded joint was studied. At the same time, the influence of HAZ width on the distribution of stress triaxiality in welded joint was studied in each strength match condition. The results indicate that the stress state in welded joints with different weld strength matches was complicated, compared to the base material. Bounce in the stress traxiality existed in the boundary between the base material and HAZ and between the weld and HAZ. The maximum of stress traxiality in high strength match welded joint was the largest. On the contrary, the maximum of stress traxiality in low strength match welded joint was the least. Under the condition of equal strength match, the position of the maximal stress traxiality changed from the boundary between the base material and HAZ to the boundary between the weld and HAZ with the increasing of the width of HAZ. Under the condition of high strength match, the maximum of stress traxiality appeared in the boundary between the weld and HAZ, and the maximum of stress traxiality reduced gradually with the increasing of the width of HAZ. However, under the condition of low strength match, the maximum of stress traxiality appeared in the boundary between the base material and HAZ, and the maximum of stress traxiality also reduced gradually with the increasing of the width of HAZ.

Key words: aluminum alloy welded joint; strength match; HAZ; stress triaxiality; FEA

A control technique for electron-beam scan welding WEI Shouqi, LI Xuejiao, MO Jinhai (College of Mechanical & Electrical Engineering, Guilin University of Electronic Technology, Guilin 541004, China). pp 89 – 92, 96

Abstract: In electron-beam (EB) scan welding, the 2D seam tracking could be approximated by combination of limited line segments and basic arc graphics, hence the whole welding processes could be divided into 3 steps: tracing of teaching, calculating of tracking data, and scan welding. In these processes, three main problems, non-vertical of x-y scanning axis, distortion of scanning track and defocusing of EB spot could be solved by proper conversion of oblique and rectangular coordinates, dynamic correction of deflection scanning magnetizing current with EB's deflection amplitude and velocity, and dynamic correction of focusing magnetizing current with EB's deflection vector, respectively. The welding results with "track & field" type seam tracking reveal that, eccentric distance is above 0.08 mm, depth error is lower than 0.13 mm, width error in surface is lower than 0.16 mm. The proposed welding method could precisely repeat the seam tracking and obtain excellent welding quality.

Key words: electron-beam scan welding; coordinate conversion; scanning track distortion; electron-beam spot defocusing

Test and analysis on corrosion resistance of MWEDM surfaces ZHANG Bin[1,2], GUO Libin[1], CUI Hai[1,3], ZHANG Huigang[1] (1. College of Mechanical and Electrical Engineering, Harbin Engineering University, Harbin 150001, China; 2. Library, Harbin Engineering University, Harbin 150001, China; 3. Engineering Training Center, Harbin Engineering University, Harbin 150001, China). pp 93 – 96

Abstract: In order to understand the corrosion resistance of different materials surfaces machined by micro wire electrical discharge machining (MWEDM), the specimens of three kinds of materials, including W18Cr4V, 60Si2Mn and M42, were separately processed. The micro electrolytic cell equipment and electrochemical workstation were applied to test the corrosion resistance of specimen surfaces, and the electrochemical impedance spectroscopy and potentiodynamic polarization curves were measured and analyzed. Besides, the surfaces after corrosion were observed with inverted metallurgic microscope, and were compared to flat grinding surfaces. The results showed that corrosion resistance of MWEDM surfaces was superior to that of flat grinding surfaces. For different materials, corrosion resistance of MWEDM surfaces was significantly different from each other. For the same material, the surface with better corrosion resistance could be obtained by using appropriate processing parameters.

Key words: micro wire electrical discharge machining; corrosion resistance; electrochemical impedance spectroscopy; potentiodynamic polarization curve

Using dynamic induction heating to inhibit martensite structure formed in heat-affected zone of U71Mn steel rail after surface welding YAN Wentao, LI Xiaoyan, LI Hui, SUN Jiantong (School of Material Science and Engineering, Beijing University of Technology, Beijing 100124, China). pp 97 – 100, 108

Abstract: A dynamic induction heating method was used to inhibit the formation of martensite in heat-affected zone (HAZ) of U71Mn steel rail after surface welding. The inhibition of martensite structure was characterized by optical microstructure analysis and microhardness testing. The experimental results showed that when the U71Mn steel rail was welded in cold welding condition, cracks would form directly in the heat-affected zone, and the microstructure was martensite. With the increase of preheating and post-heating temperature, the amount of martensite reduced significantly. When the preheating temperature was 320 ℃ and post-heating temperature was 550 ℃, the martensite structure could be inhibited completely, and the heat-affected zone consisted of sorbite structure whose size was smaller than pearlite structure in the base metal. The microhardness of the heat-affected zone also distributed uniformly.

Key words: dynamic induction heating; U71Mn steel rail; surface welding; martensite

Arc pressure analysis in variable polarity TIG welding CHENG Lin, HU Shengsun, WANG Zhijiang (Tianjin Key Laboratory of Advanced Joining Technology, Tianjin University, Tianjin 300072, China). pp 101 – 104

Abstract: The arc pressure during horizontal variable polarity gas tungsten arc welding (VPTIG) was measured by pressure transducer under different welding conditions. The radial distribution of arc pressure was investigated, and the central arc pressures for DC TIG welding and VPTIG welding with a period of 5% and 15% for direct current electrode positive (DCEP) were compared. The experimental results showed that the radial distribution of VPTIG pressure was hyperbolic. When the welding current was in the range of 100 A to 140 A and with the same root mean square value, the arc pressure decreased gradually with the increase of time ratio of DCEP at one cycle during DC TIG welding and VPTIG welding with a period of 5% and of 15% for DCEP, due to the difficulties of electron emission and arc divergence in the period of DCEP. And the integrated arc force was directly proportional to the square of welding current.

Key words: hyperbolic distribution; arc pressure; horizontal welding; variable polarity gas tungsten arc welding

Effect of hot-cutting defect on reliability of brazing process in ceramic package manufacturing——II. Brazing structure design ZENG Chao, WANG Chunqing, TIAN Yanhong, ZHANG Wei (State Key Lab of Advanced Welding and Joining, Harbin Institute of Technology, Harbin 150001, China). pp 105 – 108

Abstract: Reliability of brazing process in ceramic package manufacturing depends on the interaction between thermal stress induced by mismatch of CTE (coefficient of thermal expansion) and defect in ceramic generated in the process before brazing. This paper based on the feature that defects with different degrees of danger spatially locate differently, and employed ANSYS software to analyze the distribution of the thermal stress in brazing process. A novel idea of avoiding the stress locating at defect region was applied to improve the reliability of assembly process. This idea is different from the traditional optimizing method to lowering the stress over the whole component, and is more flexible for the package design, and it is also more effective for improving the reliability of ceramic package manufacturing.

Key words: thermal mismatch; package structure; process reliability

Finite element numerical simulation of electron beam welding of TC4 titanium alloy ZENG Qingji[1], XU Lianyong[1,2], HAN Yongdian[1,2], JING Hongyang[1,2], ZHOU Chunliang[3] (1. School of Materials Science and Engineering, Tianjin University, Tianjin 300072, China; 2. Tianjin Key Laboratory of Advanced Joining Technology, Tianjin 300072, China; 3. The 18th Research Institute of CETC, Tianjin 300381, China). pp 109 – 112

Abstract: The optimized welding parameters for electron beam welding of 9 mm thick TC4 titanium alloy plate were obtained. A finite element model was established based on ABAQUS software, and the simulated results of the weld appearance and residual stress on the weld surface agreed well with the experimental results. This proved that the combined heat source with highly penetrating cone heat source and highly irradiative dual-ellipsoid heat source could characterize the electron beam welding. Further simulated results showed that high residual stress occurred around the weld, especially, dangerous three-dimensional tensile stress existed within the weldment.

Key words: electron beam welding; TC4 titanium; finite element numerical simulation; residual stress; composite heat source